Available online at www.sciencedirect.com
SCIENCE DIRECT®
Journal of Colloid and Interface Science 272 (2004) 10–20
JOURNAL OF Colloid and Interface Science
www.elsevier.com/locate/jcis

Influence of mesoporosity on the sorption of 2,4-dichlorophenoxyacetic acid onto alumina and silica

Keith W. Goyne,[a,b] Jon Chorover,[b,*] Andrew R. Zimmerman,[c] Sridhar Komarneni,[a,d] and Susan L. Brantley [c]

[a] *Department of Crop and Soil Sciences, The Pennsylvania State University, 116 A.S.I. Bldg., University Park, PA 16802, USA*
[b] *Department of Soil, Water and Environmental Science, University of Arizona, 429 Shantz Building, Tucson, AZ 85721-0038, USA*
[c] *Department of Geosciences, The Pennsylvania State University, 239 Deike Bldg., University Park, PA 16802, USA*
[d] *Materials Research Institute, The Pennsylvania State University, 205 M.R.L. Bldg., University Park, PA 16802, USA*

Received 1 May 2003; accepted 12 December 2003

Abstract

Two SiO_2 and three Al_2O_3 adsorbents with varying degrees of mesoporosity (pore diameter 2–50 nm) were reacted with 2,4-dichlorophenoxyacetic acid (2,4-D) at pH 6 to investigate the effects of intraparticle mesopores on adsorption/desorption. Anionic 2,4-D did not adsorb onto either SiO_2 solid, presumably because of electrostatic repulsion, but it did adsorb onto positively charged Al_2O_3 adsorbents, resulting in concave isotherms. The Al_2O_3 adsorbent of highest mesoporosity consistently adsorbed more 2,4-D per unit surface area than did the nonporous and less mesoporous Al_2O_3 adsorbents over a range of initial 2,4-D solution concentrations (0.025–2.5 mM) and reaction times (30 min–55 d). Differences in adsorption efficiency were observed despite equivalent surface site densities on the three Al_2O_3 adsorbents. Hysteresis between the adsorption/desorption isotherms was not observed, indicating that adsorption is reversible. Attenuated total reflectance-Fourier transform infrared (ATR-FTIR) spectroscopy studies confirm that 2,4-D adsorption does not occur via ligand exchange, but rather via electrostatic interaction. The results indicate that adsorbent intraparticle mesopores can result in consistently greater 2,4-D adsorption, but the amount adsorbed is dependent upon surface charge and the presence of adsorbent mesoporosity. The data also suggest that when mineral pores are significantly larger than the adsorbate, they do not contribute to diffusion-limited adsorption/desorption hysteresis. Adsorbent transformations through time are discussed.

Keywords: Mesoporosity; X-ray diffraction; Mineral transformation; 2,4-D; Adsorption/desorption isotherms; Freundlich isotherm; Frumkin–Fowler–Guggenheim isotherm; ATR-FTIR spectroscopy; Mineral–organic interactions

1. Introduction

Nanometer-sized pores within mineral particles (i.e., intraparticle pores) are thought to contribute to retention of labile natural organic matter and organic pollutants in soils and sediments [1–4]. Sorption into pores diminishes the efficacy of chemical extraction and reduces the bioavailability of such compounds [2,5–7]. Studies of hydrophobic organic contaminants (HOCs) indicate that several physical and chemical mechanisms, including increased adsorption energy resulting from compound interaction within pores, may enhance HOC retention in mineral micropores with a diameter (D_{pore}) < 2 nm [6]. Although hydrophobic micropores are likely important for HOC adsorption [8–10], hydrophilic porous surfaces may also be significant, since steric effects, slow diffusion, and tortuosity may inhibit desorption [2,6,11]. However, the effects of hydrophilic mineral pore walls on sorption of polar organic compounds are not clear. In addition, it is uncertain how mineral transformations through time will affect adsorbent mesoporosity and organic compound sorption processes.

Recent ab initio calculations indicate that sorption is most favorable in micropores that are minimally small enough to accommodate an organic compound, and this effect may contribute to contaminant persistence in the environment [4]. However, we postulated that mesopores with pore diameter (D_{pore}) equal to 2–50 nm will also affect sorption/desorption of organic compounds because fabricated intraparticle meso-

* Corresponding author.
E-mail address: chorover@cals.arizona.edu (J. Chorover).

0021-9797/$ – see front matter
doi:10.1016/j.jcis.2003.12.040

porous adsorbents effectively remove organic compounds and heavy metals from contaminated waters [12–19]. Other evidence also supports the likelihood that mineral mesopores may enhance organic compound sorption processes. For instance, the structure of water in close proximity to mineral surfaces differs from that in the bulk [20]. This may create favorable conditions for contaminant sorption within mesopores, even though the extent of structured water may not permeate throughout a mesopore as it apparently does within a micropore [4]. In addition, Pignatello [21] suggests that contaminant/pore interactions facilitate capillary condensation of organics within geosorbent pores, and Mastral et al. [22] reported that increasing the number of benzene rings in polynuclear aromatic compounds results in more favorable sorbate/sorbate interactions within mesopores. More recently, Zimmerman et al. [23] observed that nitrogeneous organic compouds smaller than one-half mesopore diameter exhibited significantly greater surface area-normalized adsorption to mesoporous alumina and silica, relative to nonporous analogues.

Prior research on intraparticle porosity has focused primarily on adsorption of HOCs, and not on the adsorption of polar and/or ionic contaminant compounds, such as the acidic pesticide 2,4-dichlorophenoxyacetic acid (2,4-D). Thus, additional research is necessary to elucidate the interaction of these types of compounds in the presence and absence of intraparticle mesopores. Given that mesoporous materials may be poorly crystalline solids [14,18], it is also necessary to document any changes in adsorbent characteristics (e.g., surface area, mean pore diameter, crystal structure) as a function of reaction time in solution. If significant changes occur, these may affect long-term sorption/desorption reactions [24] and inhibit application of mesoporous adsorbents for engineered remediation. Whereas some data on the stability of MCM-41 and MCM-48 are available [14,25,26], the long-term stability of calcined materials and neutral-templated mesoporous alumina has not been documented previously for aqueous suspensions.

The herbicide 2,4-D, which is widely used in agriculture, may be quite mobile in aqueous systems because of its acidic carboxyl group ($pK_a = 2.80$ [27,28]), which imparts a negative charge throughout a wide pH range in natural waters. Previous 2,4-D sorption research has shown that low herbicide affinity for Na-, K-, or Ca-saturated 2:1 and 1:1 layer type silicates is due to anion repulsion [28–32]. However, Fe saturation, Fe oxide coatings, and increased loading of $Al(OH)_x$ species on the montmorillonite surface yields significantly enhanced 2,4-D adsorption [28,30,31]. Sorption of 2,4-D onto iron and aluminum oxides is favored when solution pH is below the adsorbent point of zero net charge (PZNC) and above the pK_a of the adsorptive compound [31–34].

Most batch sorption studies investigating 2,4-D uptake and retention have observed L- or C-type sorption isotherms [29,30,33,35–37]. However, S-type or concave isotherms have been observed for sorption onto Fe-saturated montmorillonite [28], ferrihydrite [31], whole soils [32], and lignin [35]. It is hypothesized that S-type isotherms result from a combination of electrostatic attraction and intermolecular van der Waals forces, the latter associated with mutual interactions of aromatic moieties of 2,4-D that become increasingly important with increasing surface coverage [31,32,34,38]. The rate of 2,4-D sorption is rapid; equilibrium is reached on the order of minutes to hours [29,30,32,39], although sorption reversibility is highly dependent upon adsorbent chemistry [28,30–32,35].

The objectives of this research were to (a) determine the effects of mineral mesopores on the adsorption and retention of 2,4-D to alumina and silica adsorbents, (b) elucidate the bonding mechanism of 2,4-D to the adsorbents, and (c) document mesoporous adsorbent transformation as a function of reaction time in suspension as it affects objectives (a) and (b).

2. Materials and methods

2.1. Adsorbent synthesis and treatment

Five mineral adsorbents were used in the present work: (1) mesoporous Al_2O_3 (Al-P_{242}), (2) less mesoporous Al_2O_3 (Al-P_{141}), (3) nonporous Al_2O_3 (Al-NP_{37}), (4) mesoporous SiO_2 (Si-P_{1570}), and (5) nonporous SiO_2 (Si-NP_8), where the subscripts refer to specific surface area in $m^2\,g^{-1}$. Al-NP_{37} and Si-NP_8 were purchased from Alfa Aesar (Ward Hill, MA), stock numbers 40007 and 89709, respectively. Al-NP_{37} was washed and dried as described in Goyne et al. [40] to remove an N-containing soluble constituent associated with synthesis. Al-P_{141} was prepared from boehmite supplied by the CONDEA Vista Co. (Houston, TX) and is sold under the trade name Disperal. This mineral was calcined at 723 K for 24 h to induce dehydroxylation. Al-P_{242} and Si-P_{1570} were prepared using a neutral template route and a cationic template route, respectively [41–43]. The synthesis procedure and removal of the templates from the fabricated adsorbents is detailed elsewhere [40,41]. All minerals, except Si-NP_8, were ground gently prior to characterization and stored in polyethylene bottles prior to use.

2.2. Adsorbent characterization techniques

Pore structure and specific surface area of pre- and postreacted adsorbents were examined using N_2 sorptometry (ASAP 2010, Micromeritics). Samples (0.5–2 g) were outgassed for at least 6 h (423 K, 5 μm Hg) prior to analysis, and adsorption/desorption isotherms were measured at 77 K. Specific surface area (S_{BET}) was estimated using multipoint adsorption data from the linear segment of the N_2 adsorption isotherms [44] in the relative pressure range 0.05–0.2 using Brunauer–Emmett–Teller (BET) theory. Pore size distributions were calculated from adsorption branch isotherms according to the Barrett–Joyner–Halenda (BJH) method [45],

assuming right cylindrical pores closed on one end and using the Halsey layer thickness equation [46].

Powder X-ray diffraction (XRD) analyses were conducted on randomly oriented, back-filled 15×5 mm circular samples mounted in spinning holders. All patterns were collected using a Philips X'pert MPD diffractometer equipped with a spinning stage and an X'Celerator multiple strip detector using Ni-filtered CuK_α radiation at 50 kV and 40 mA. Data were collected in continuous scan mode from 3° to 80° 2θ, with a step size of 0.017° and a divergent slit of 0.0625°. TEM images (Philips EM420ST) confirmed the presence of mesoporosity in the samples.

Thermal gravimetric analyses (TGA) and differential thermal analyses (DTA) were conducted simultaneously for unreacted and reacted samples to quantify mineral transformation (Setaram TG92). Samples were heated at a rate of $10\,^{\circ}\mathrm{C\,min^{-1}}$ from 25 to 1000 °C and then cooled to room temperature at an equivalent rate. After cooling to ambient temperature, the sample was analyzed (without opening the system) for background subtraction.

2.3. Batch adsorption and desorption experiments

Mineral adsorbents were suspended in a 0.02 M $CaCl_2$ background electrolyte solution to give a sorbent-surface-area-to-solution ratio of 2.86×10^3 $\mathrm{m^2\,l^{-1}}$ in PTFE centrifuge tubes. The solution also contained 200 $\mathrm{mg\,l^{-1}}$ $HgCl_2$ to inhibit microbial activity [47]. All sorption experiments were conducted in the absence of pH buffers to prevent competitive sorption between buffer constituents (e.g., phosphate) and 2,4-D for available sorption sites [34] and to allow measurement of pH shifts that could indicate the occurrence of ligand exchange reactions [48]. Solutions of 0.06 M HCl or 0.02 M $Ca(OH)_2$ were added to yield a final pH of 5.5 for SiO_2 and pH 6.0 for Al_2O_3 after 24 h of reaction. Samples were spiked with analytical grade 2,4-D (chemical purity > 98%) dissolved in 0.02 M $CaCl_2$ to give concentrations ranging from 0 to 2.5 mM. Samples were then placed on an end-over-end shaker (7 rpm) in the dark at 298 K for reaction times ranging from 30 min to 55 d. Adsorbent-free controls (no mineral) were reacted concurrently to measure compound loss resulting from sorption to centrifuge tube walls, volatilization or transformation. None of these were found to be significant.

At the end of the reaction period, mineral suspensions were centrifuged at 15,290g and 298 K for 40 min. An aliquot of supernatant solution was removed by pipette for measurement of 2,4-D concentration by high-performance liquid chromatography (HPLC) on a reverse-phase (Hypercarb, ThermoQuest) column followed by detection at 280 nm within 24 h (Waters Inc., equipped with a photodiode array (PDA) detector; 85% acetonitrile: 0.15% trifluoroacetic acid was used as a mobile phase at a flow rate of $2\,\mathrm{ml\,min^{-1}}$). Surface excess of 2,4-D was calculated as:

$$\Gamma_{\mathrm{ads}} = \frac{C_{\mathrm{ads},B} - C_{\mathrm{ads},S}}{SA_S}, \tag{1}$$

where Γ_{ads} is the surface excess after the adsorption period ($\mu\mathrm{mol\,m^{-2}}$), $C_{\mathrm{ads},S}$ and $C_{\mathrm{ads},B}$ are the equilibrium 2,4-D concentrations in supernatant solutions of mineral suspensions (S) after reaction ($\mu\mathrm{mol\,kg^{-1}}$) and in the corresponding blank (B), and SA_S is the suspension concentration of adsorbent ($\mathrm{m^2\,kg^{-1}}$). The remaining supernatant solution was aspirated into amber vials for determination of pH using a calibrated Orion Ross semimicro combination pH electrode attached to a Beckman Φ390 pH meter. Concentrations of Al were measured by atomic absorption (AA) spectrophotometry (IL Video 22, Allied Analytical Systems) or magnetic sector inductively coupled plasma mass spectrometry (ICP-MS, Finnigan ELEMENT).

Desorption experiments were initiated immediately after the adsorption step by adding a mass of 0.02 M $CaCl_2$, containing 200 $\mathrm{mg\,l^{-1}}$ $HgCl_2$, equivalent to the mass of supernatant solution removed. Desorption reaction times were equal to those for adsorption. At the end of a given desorption period, supernatant solutions were again aspirated and analyzed. The adsorbate retention was calculated from Eq. (2),

$$\Gamma_{\mathrm{des}} = \Gamma_{\mathrm{ads}} - \left\{ \frac{(C_{\mathrm{des},S})(M_{\mathrm{tot,soln}}) - (C_{\mathrm{ads},S})(M_{\mathrm{ent}})}{SA} \right\}, \tag{2}$$

where Γ_{des} is the surface excess of 2,4-D ($\mu\mathrm{mol\,m^{-2}}$) remaining on the surface after the desorption step, $C_{\mathrm{des},S}$ is the equilibrium 2,4-D concentration in supernatant solutions of mineral suspensions (S) after the desorption reaction ($\mu\mathrm{mol\,kg^{-1}}$), $M_{\mathrm{tot,soln}}$ is the total mass of solution (kg) in the reaction vessel during desorption, M_{ent} is the mass of entrained solution (kg) remaining in the adsorbent pellet after aspiration of adsorption phase supernatant, and SA is the total surface area of the adsorbent ($\mathrm{m^2}$) in the reaction vessel. The mass of entrained solution is determined by mass balance (Eq. (3)),

$$M_{\mathrm{ent}} = (M_{\mathrm{tot,asp}}) - (M_{\mathrm{vessel}} + M_{\mathrm{adsorbent}}), \tag{3}$$

where $M_{\mathrm{tot,asp}}$ is the total mass (kg) after aspiration of adsorption phase supernatant solution (i.e., mass of reaction vessel, adsorbent, and entrained solution), M_{vessel} is the mass of the reaction vessel, and $M_{\mathrm{adsorbent}}$ is the initial mass of adsorbent added to the reaction vessel. After a selected number of desorption steps, the pellet was recovered for analysis of mineral transformation and ethanol was added to displace entrained solution. After resuspension of the adsorbent pellet in ethanol, samples were centrifuged at 28,000g for 15 min at 298 K. The ethanol was then aspirated and this procedure was repeated two more times. Samples were then placed in an oven at 313 K for 48 h. Dried solid samples were stored in a desiccator prior to further analysis.

2.4. Infrared spectroscopy

Attenuated total reflectance (ATR) Fourier transform infrared (FTIR) spectroscopy was employed to investigate the mechanism of 2,4-D adsorption. Samples were prepared and

reacted for 24 h at initial 2,4-D concentrations of 0 and 3.5 mM, as described previously, except that these suspensions contained no $HgCl_2$. After adsorption, samples were centrifuged and ca. 3.0 ml of supernatant solution was left in the suspension to create a slurry. ATR-FTIR slurry samples were immediately transferred into an ATR cell equipped with a 45° ZnSe flat plate crystal (ARK cell, Thermo Spectra-Tech, Inc.), and spectra were obtained by averaging 400 scans at 2 cm^{-1} resolution on a Nicolet Magna 560 spectrometer. An initial spectrum was collected, followed by subsequent spectra after sample drying in CO_2 and H_2O free air at cumulative drying times of 3, 5, 7, 9, 18, and 24 h. The pH values and 2,4-D concentrations of supernatant solutions were measured as indicated above.

3. Results and discussion

3.1. Solid-phase characterization of adsorbents

Studies pertaining to surface charge and site density for these adsorbents are published elsewhere [40], and a summary of selected data is provided in Table 1. Powder XRD patterns for unreacted adsorbents are consistent with η-Al_2O_3 (Ref. code 04-0875) for Al-P_{242} and Al-P_{141} and γ-Al_2O_3 (Ref. code 10-0425) for Al-NP_{37}, in the International Center for Diffraction Data (ICDD) database. Transmission electron microscopy confirmed the presence of wormhole-like pores in the adsorbents synthesized by the neutral template pathway [40].

3.2. Adsorption and desorption of 2,4-D

Adsorption of 2,4-D to Si-NP_8 and Si-P_{1570} was not significantly different from zero. At the mean experimental pH (pH 5.1 and 5.9 for Si-NP_8 and Si-P_{1570}, respectively), Γ_- (surface excess of Cl^-) values for these solids are near zero or very slightly negative (Table 1). In this pH range, the carboxyl group of 2,4-D is dissociated and likely also excluded from the surface by charge repulsion from dissociated silanol sites. However, given that significant proton dissociation from these silica phases is initiated only at alkaline pH (>7) [40], our results indicate a lack of adsorption to a near neutrally charged surface. Evidently, the high polarity of 2,4-D and the hydrophilic silica surface make adsorption to the Si solids unfavorable energetically.

In contrast, the pesticide did adsorb to positively-charged Al_2O_3 surfaces (Figs. 1a–1e; Table 2) and Al-P_{242} consistently adsorbed more 2,4-D than did Al-P_{141} or Al-NP_{37} (Figs. 1a–1d; Table 2) at a given equilibrium concentration. Given that the error bars indicate 95% confidence intervals, it is evident that sorption is increased significantly due to greater intraparticle porosity. At the highest initial concentration of 2,4-D (2.5 mM), Al-P_{242} sorbed on average 27% and 17% more herbicide than did Al-NP_{37} and Al-P_{141}, respectively. In contrast, Al-P_{141} and Al-NP_{37} adsorbed comparable amounts of 2,4-D except at the highest suspension concentration, where Al-P_{141} adsorbed 11% more herbicide. Even at the highest surface excess of 2,4-D, the quantity sorbed is significantly lower than the surface excess of Cl^- retained in the absence of 2,4-D (Γ_-). This is despite the fact that the compound is anionic at the experimental pH. Assuming 2,4-D sorbs only to positively charged ($\equiv AlOH_2^+$) sites, then at the highest initial 2,4-D concentration, sorbate molecules occupied 21, 28, and 45% of these sites for Al-NP_{37}, Al-P_{141}, and Al-P_{242}, respectively.

Sorption of 2,4-D to the alumina adsorbents was fit to the Freundlich equation to provide a concise set of parameters for comparison of sorbent affinity,

$$\Gamma_{ads} = AC_{ads}^{n}, \tag{4}$$

where parameters A and n are the intercept and slope, respectively, in a log–log plot of 2,4-D adsorption isotherm data. Isotherms were nonlinear with $n > 1$ (i.e., concave isotherm) for almost all reaction periods (Table 3). Adsorption isotherms of 2,4-D with this shape are postulated to reflect enhanced surface affinity with increasing surface coverage due to favorable adsorbate/adsorbate interaction [28,31,49]. Similar isotherms have been observed

Table 1
Physical characteristics and surface charge properties of the adsorbents

Adsorbent	S_{BET} ($m^2\,g^{-1}$)	D_{pore} (nm)	S_{ip} ($m^2\,g^{-1}$)	PZNC	pKa_1	pKa_2	Γ_+ ($\mu mol\,m^{-2}$)	Γ_- ($\mu mol\,m^{-2}$)	$\Delta\Gamma$ ($\mu mol\,m^{-2}$)
Si-P_{1570}	1570 ± 19	2.3 ± 0.5	1565 ± 19[a]	<2.85	NA	6.85 ± 0.63	0.1 ± 0.17	−0.03 ± 0.06	0.07 ± 0.18
Si-NP_8	7.5 ± 0.1	14 ± 3	NA	<2.82	NA	7.74 ± 0.27	0.0 ± 0.26	−0.08 ± 0.06	0.08 ± 0.27
Al-P_{242}	242 ± 4	8.2 ± 0.4	234 ± 4	6.47 ± 0.05	6.19 ± 0.62	6.93 ± 0.78	0.5 ± 0.29	0.91 ± 0.09	−0.41 ± 0.30
Al-P_{141}	141 ± 6	9.6 ± 0.4	131 ± 6	6.87 ± 0.05	6.07 ± 0.75	6.74 ± 1.20	0.0 ± 0.32	0.9 ± 0.10	−0.9 ± 0.33
Al-NP_{37}	37 ± 2	20 ± 2	NA	6.66 ± 0.06	6.58 ± 0.67	7.14 ± 0.83	0.6 ± 0.12	0.9 ± 0.17	−0.3 ± 0.17

Note. See Goyne et al. [37] for detailed methods and data analysis; S_{BET} is the specific surface area ±95% C.I. as measured by N_2 BET; D_{pore} is the mean pore diameter ±95% C.I. determined by the BJH method on the adsorption isotherm leg; S_{ip} is the intraparticle surface area (within pores 2–20 nm diameter) ±95% C.I. determined by BJH method; PZNC is the point of zero net charge ±95% C.I; values of PZNC not encountered in the pH range of the experiment are expressed as < the lowest pH values of experiment; pKa_1 and pKa_2 are surface acidity equilibrium constants calculated using $\Delta\Gamma$ values from [37]; Γ_+ is the value for Ca^{2+} adsorption ±95% C.I. at average experimental pH; Γ_- is the value for Cl^- adsorption ±95% C.I. at average experimental pH; $\Delta\Gamma = (\Gamma_+ - \Gamma_-)$; NA is not applicable.

[a] Based on values reported in Goyne et al. [37] for Si-P_{700}, which is a less porous material produced using cationic template procedure (i.e., the value is a conservative estimate).

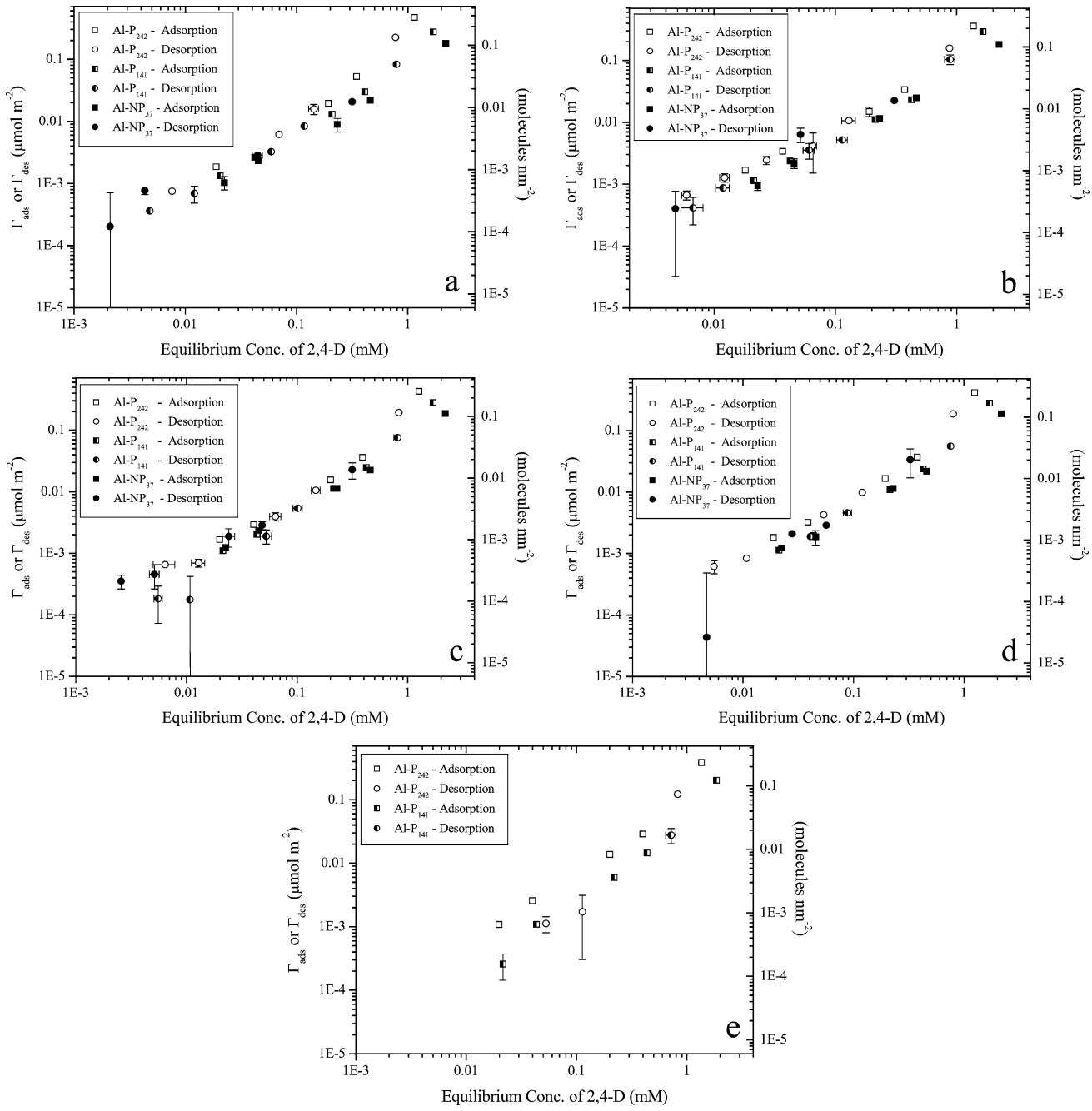

Fig. 1. 2,4-D sorbed on Al-P_{242}, Al-P_{141}, and Al-NP_{37} after adsorption (Γ_{ads}) or desorption (Γ_{des}) reaction. Reaction times were (a) 30 min, (b) 1 d, (c) 3 d, (d) 5 d, and (e) 55 d (duplicate or triplicate means are shown and error bars, where larger than symbol, represent 95% C.I.).

for 2,4-D adsorption onto Fe-saturated Wyoming montmorillonite [28], ferrihydrite [31], and Georgeville B horizon soil [32].

The contribution of lateral sorbate/sorbate interaction at the surface was modeled with the Frumkin–Fowler–Guggenheim (FFG) equation [50],

$$\frac{\theta}{1-\theta}e^{2\theta a} = \beta C_{\text{ads}}, \tag{5}$$

where θ is the adsorbate surface excess ($\text{mol}\,\text{m}^{-2}$) normalized to the total number of available anion adsorption sites (Γ_{-}; $\text{mol}\,\text{m}^{-2}$) at the experimental pH, a is the lateral interaction coefficient, and β is the adsorption constant. Values of $a < 0$ are consistent with attractive lateral sorbate/sorbate interactions, whereas $a > 0$ suggest repulsive lateral interactions. If $a = 0$ then Eq. (5) reduces to the Langmuir equation. The values for a and β were determined by plotting $\log[\theta/(1-\theta)C]$ versus θ, where a is the slope of the resulting straight line and $\log\beta$ is the intercept [51]. Results from fitting experimental data to the FFG equation (Table 4; Figs. 2a–2c) are consistent with an attractive lateral interaction coefficient for 2,4-D sorbed to

Table 2
Percentage of 2,4-D adsorbed onto mineral surface as a function of time and initial 2,4-D concentration

Time	Adsorbent	Initial concentration of 2,4-D (mM)				
		2.5	0.5	0.25	0.05	0.025
30 min	Al-NP_{37}	20.4 ± 0.2	12.4 ± 0.3	10 ± 3	13.6 ± 0.9	12 ± 3
	Al-P_{141}	31.8 ± 0.8	17.4 ± 0.5	15.3 ± 0.1	15.3 ± 0.9	16 ± 1
	Al-P_{242}	53.8 ± 0.1	30.4 ± 0.1	22.4 ± 0.2	–	22 ± 2
1 d	Al-NP_{37}	20.6 ± 0.3	13 ± 1	10.3 ± 0.6	14 ± 2	12 ± 2
	Al-P_{141}	31.7 ± 0.2	17.2 ± 0.4	15.2 ± 0.4	15.1 ± 0.6	16 ± 1
	Al-P_{242}	40.9 ± 0.3	19.4 ± 0.4	17 ± 3	19.8 ± 0.3	20 ± 1
3 d	Al-NP_{37}	21 ± 1	13.0 ± 0.1	13.1 ± 0.5	13.6 ± 0.7	15 ± 1
	Al-P_{141}	32 ± 2	14.4 ± 0.1	13.1 ± 0.2	12 ± 1	13 ± 1
	Al-P_{242}	48.9 ± 0.2	20.9 ± 0.2	18.1 ± 0.3	17.1 ± 0.6	19.7 ± 0.8
5 d	Al-NP_{37}	22 ± 2	12.6 ± 0.1	13.1 ± 0.3	11 ± 3	14 ± 1
	Al-P_{141}	31.9 ± 0.3	13.7 ± 0.2	12.6 ± 0.4	11 ± 1	13 ± 1
	Al-P_{242}	47.6 ± 0.2	21.4 ± 0.1	19.4 ± 0.1	18.8 ± 0.4	21 ± 1
55 d	Al-NP_{37}	–	–	–	–	–
	Al-P_{141}	23.8 ± 0.2	8.7 ± 0.2	7.2 ± 0.1	6.7 ± 0.6	3 ± 2
	Al-P_{242}	44.8 ± 0.3	17.1 ± 0.2	16.4 ± 0.1	16 ± 1	13.5 ± 0.2

Note. Percentage of 2,4-D adsorbed ±95% C.I. Adsorption values were calculated from mass lost from solution.

Table 3
Freundlich parameters for Al_2O_3 isotherms

Time	Parameter	Al-NP_{37}		Al-P_{141}		Al-P_{242}	
		Adsorption	Desorption	Adsorption	Desorption	Adsorption	Desorption
30 min	log A ± 95% C.I.	−3.9 ± 0.34a†	−5.3 ± 0.77b†	−3.4 ± 0.33ac†	−3.8 ± 0.34ac†	−2.6 ± 0.86c†	−3.0 ± 0.74ac†
	n ± 95% C.I.	1.09 ± 0.09a†	0.7 ± 0.17b†	1.18 ± 0.09a†	1.08 ± 0.08a†	1.3 ± 0.23a†	1.2 ± 0.18a†
	R^2 (n)	0.98 (15)	0.90 (12)	0.99 (15)	0.99 (15)	0.97 (8)	0.98 (8)
1 d	log A ± 95% C.I.	−3.8 ± 0.17a†	−3 ± 1.3a§	−3.3 ± 0.49a†	−3.79 ± 0.46a†	−3.3 ± 0.51a†	−3.7 ± 0.72a†
	n ± 95% C.I.	1.13 ± 0.04a†	1.2 ± 0.27a§	1.2 ± 0.13a†	1.1 ± 0.11a†	1.2 ± 0.13a†	1.1 ± 0.17a†
	R^2 (n)	1.0 (15)	0.88 (14)	0.97 (15)	0.97 (15)	0.97 (15)	0.94 (15)
3 d	log A ± 95% C.I.	−4.0 ± 0.23ac†	−4.7 ± 0.50a†§	−3.3 ± 0.41b†	−3 ± 1.3ab†	−2.9 ± 0.59b†	−3.3 ± 0.63bc†
	n ± 95% C.I.	1.08 ± 0.03a†	0.9 ± 0.11b†§	1.2 ± 0.11ac†	1.4 ± 0.30ac†	1.3 ± 0.15c†	1.2 ± 0.15ac†
	R^2 (n)	0.99 (15)	0.96 (15)	0.98 (15)	0.89 (15)	0.96 (15)	0.96 (15)
5 d	log A ± 95% C.I.	−3.9 ± 0.30a†	−3.9 ± 0.83abc†§	−3.3 ± 0.45bc†	−3.8 ± 0.20ab†	−3.0 ± 0.56c†	−3.3 ± 0.50abc†
	n ± 95% C.I.	1.11 ± 0.08a†	1.1 ± 0.20a§	1.2 ± 0.12a†	1.11 ± 0.05a†	1.3 ± 0.15a†	1.2 ± 0.12a†
	R^2 (n)	0.99 (15)	0.95 (10)	0.98 (15)	1.0 (11)	0.96 (15)	0.97 (15)
55 d	log A ± 95% C.I.	–	–	−2.9 ± 0.46a†	4 ± 1.8b§	−2.9 ± 0.54a†	−2 ± 1.8a†
	n ± 95% C.I.	–	–	1.4 ± 0.13a†	3.6 ± 0.53b§	1.3 ± 0.14a†	1.6 ± 0.47a†
	R^2 (n)	–	–	0.98 (15)	1.0 (4)	0.97 (15)	0.89 (10)

Note. Mean values within a row followed by the same letter (a, b, c) are not significantly different ($\alpha = 0.05$); mean values for a parameter (i.e., A or n) within a column followed by the same symbol (†, §) are not significantly different ($\alpha = 0.05$); n is the number of data points used in linear regression analysis.

porous and nonporous alumina. (Plots for $a = 0$ shown in Figs. 2a–2c are included for comparative purposes only.) Although the plots suggest that porous materials have more negative a values (i.e., consistent with increased lateral attraction) than Al-NP_{37}, the difference is statistically significant only for the 3-d reaction period. Negative a values in the FFG isotherm cannot be used to as confirmation of attractive intermolecular association; verification of this mechanism can not be achieved on the basis of macroscopic isotherm data analysis. Rather, we wish to point out that our data are consistent with this hypothesis. The adsorption constant (β) is significantly greater for Al-P_{242} relative to Al-P_{141} and Al-NP_{37} for the reaction times presented in Table 4. The Freundlich adsorption constants (A) in Table 3 indicate a similar trend (i.e., affinity for Al-P_{242} > Al-P_{141} and Al-NP_{37}).

The rate of 2,4-D adsorption to Al_2O_3 is rapid (i.e., equilibrium is achieved in <30 min; Table 2). These data are in agreement with those presented in Table 3, indicating that adsorption/desorption isotherms for 2,4-D on Al_2O_3 surfaces were nearly independent of reaction time. In cases where significant differences exist in Table 3, discrepancies between the parameters may arise due to dissimilar equilibrium pH values (Table 5) and/or transformation of the adsorbent during the course of reaction. The data in Table 2 suggest that mineral transformation between 5 and 55 d may decrease the percentage of 2,4-D adsorbed when the initial herbicide concentration is very low (i.e., 0.025 mM), but the effect is less evident at higher concentrations.

Adsorption/desorption hysteresis was not observed for the Al_2O_3 adsorbents during any reaction time (Figs. 1a–1e) indicating that adsorption is reversible. That is, the presence

Table 4
Frumkin–Fowler–Guggenheim (FFG) parameters for Al_2O_3 isotherms

Time	Parameter	Al-NP_{37}	Al-P_{141}	Al-P_{242}
1 d	$\log\beta \pm 95\%$ C.I.	1.71 ± 0.03a†	1.78 ± 0.02b†	1.97 ± 0.03c†§
	$a \pm 95\%$ C.I.	-1.7 ± 0.37a†	-2.1 ± 0.12a†	-1.8 ± 0.19a†
	R^2 (n)	0.89 (15)	0.99 (15)	0.97 (15)
3 d	$\log\beta \pm 95\%$ C.I.	1.75 ± 0.02a†	1.77 ± 0.02a†	1.93 ± 0.02b†
	$a \pm 95\%$ C.I.	-1.6 ± 0.24a†	-2.1 ± 0.13b†	-1.96 ± 0.08b†
	R^2 (n)	0.94 (15)	0.99 (15)	0.99 (15)
5 d	$\log\beta \pm 95\%$ C.I.	1.71 ± 0.04a†	1.76 ± 0.02a†	1.98 ± 0.02b§
	$a \pm 95\%$ C.I.	-1.8 ± 0.44a†	-2.1 ± 0.15a†	-1.86 ± 0.09a†
	R^2 (n)	0.85 (15)	0.99 (15)	0.99 (15)

Note. Mean values within a row followed by the same letter (a, b, c) are not significantly different ($\alpha = 0.05$); mean values for a parameter (i.e., a or β) within a column followed by the same symbol (†, §) are not significantly different ($\alpha = 0.05$); n is the number of data points used in linear regression analysis.

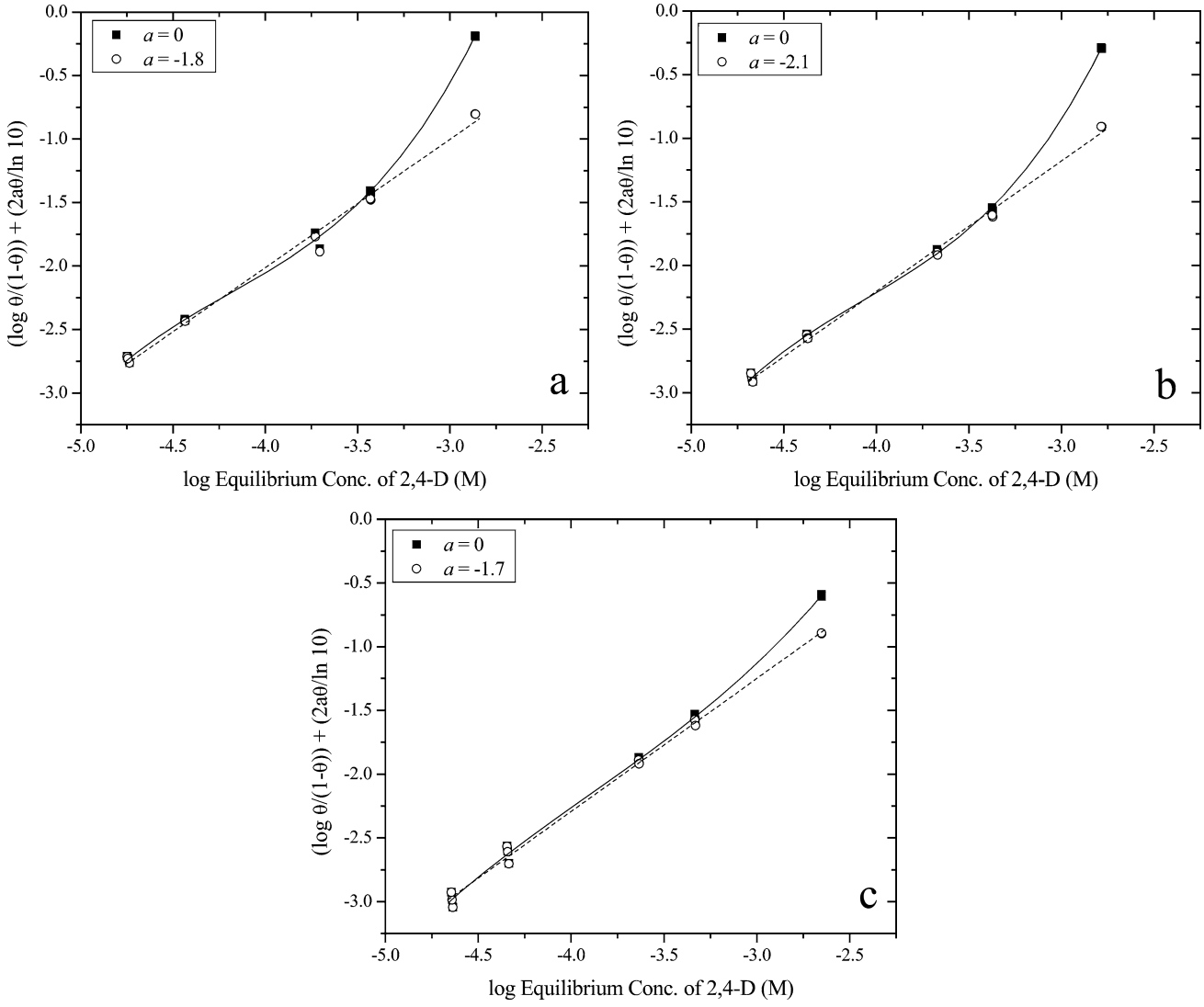

Fig. 2. Frumkin–Fowler–Guggenheim isotherms (Eq. (5)) for (a) Al-P_{242}, (b) Al-P_{141}, and (c) Al-NP_{37} at 1 d reaction time. Shown in each graph are plots of $a = 0$ (i.e., Langmuir isotherm) and $a = x$ predetermined from a plot of $\log[\theta/(1-\theta)c]$ versus θ.

of mineral mesopores did not inhibit desorption of 2,4-D. In all but a few cases, there was no statistically significant difference between adsorption and desorption Freundlich isotherm parameters for a given mineral and reaction time (Table 3). Evidently, desorption is uninhibited in these systems where D_{pore} (8–10 nm) is significantly larger than the effective size (<1 nm) of the adsorbate molecule.

Our objective was to use solids as close as possible to their postsynthetic state without addition of pH buffers. Thus, solution pH increased during the course of porous

Table 5
Final suspension pH values for Al_2O_3 experiments

Time	Al-NP_{37}		Al-$P1_{41}$		Al-P_{242}	
	Adsorption	Desorption	Adsorption	Desorption	Adsorption	Desorption
30 min	6.34 (±0.03)	6.29 (±0.03)	4.97 (±0.05)	5.85 (±0.16)	4.46 (±0.07)	4.95 (±0.07)
1 d	6.38 (±0.02)	6.30 (±0.05)	5.99 (±0.04)	6.13 (±0.03)	5.79 (±0.06)	5.92 (±0.03)
3 d	6.39 (±0.02)	6.45 (±0.02)	6.01 (±0.04)	6.18 (±0.07)	6.17 (±0.03)	6.25 (±0.05)
5 d	6.36 (±0.02)	6.12 (±0.05)	6.04 (±0.04)	6.21 (±0.06)	6.05 (±0.03)	5.92 (±0.04)
55 d	–	–	5.96 (±0.02)	6.31 (±0.02)	6.17 (±0.03)	6.19 (±0.05)

Note. pH ±95% C.I.

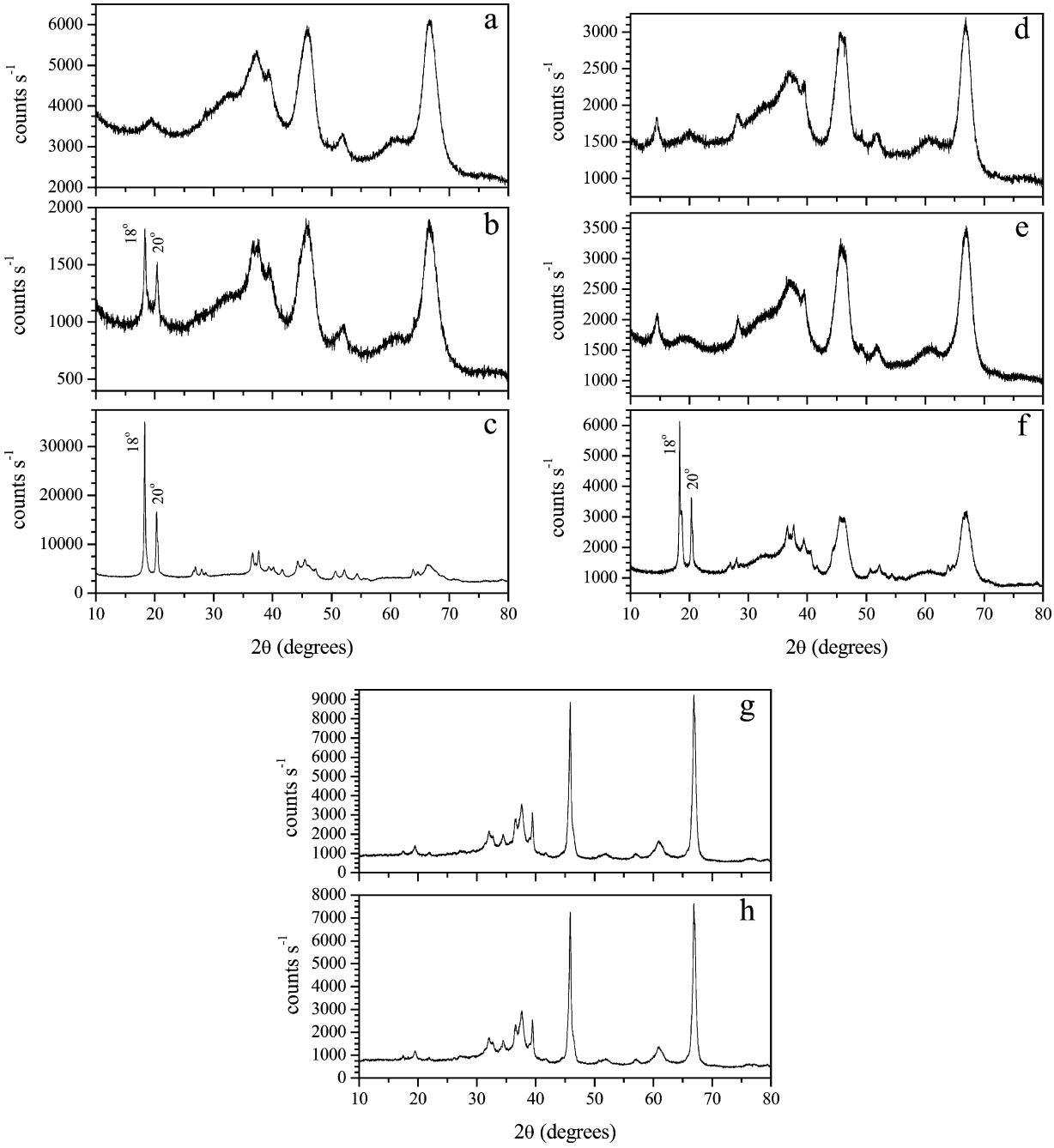

Fig. 3. Effects of adsorbent aging as observed by X-ray diffraction: (a) Al-P_{242}—0 d, (b) Al-P_{242}—9 d, (c) Al-P_{242}—165 d, (d) Al-P_{141}—0 d, (e) Al-P_{141}—9 d, (f) Al-P_{141}—165 d, (g) Al-NP_{37}—0 d, (h) Al-NP_{37}—9 d. The times listed are for adsorbent reaction time in solution.

Table 6
Changes in adsorbent characteristics—pre- versus postreaction

Adsorbent	Reaction time (d)	Change in S_{BET} (%)	Change in D_{pore} (%)	Gibbsite (mass fraction)
Al-NP_{37}	9	17*	NA	<0.01
	165	–	–	–
Al-P_{141}	9	−2	−17	<0.02
	165	17*	−8	0.15–0.18
Al-P_{242}	9	−1	−14	0.05–0.09
	165	−14*	−7	0.30–0.35

Note. S_{BET} is the specific surface area ± std. dev. as measured by N_2 BET; D_{pore} is the mean pore diameter determined by the BJH method on the adsorption isotherm leg; NA is not applicable. All pre- and postreaction samples were analyzed in duplicate or greater using N_2 adsorptometry. Values followed by (*) are significantly different from time zero ($\alpha = 0.05$). Range in mass fraction of gibbsite present in a sample was determined using TGA.

solid reaction from pH 4.5–5.0 to pH 6.0 (Table 5). This pH increase results from proton adsorption [40] and mineral transformation reactions (e.g., Fig. 3 and Table 6). Equilibrium pH stabilized at pH 6 and 6.4 after 24 h for the porous and nonporous solids, respectively. Importantly, there was no effect of 2,4-D adsorption on equilibrium pH or aluminum dissolution (data not shown). For example, after blank correction, linear regression of pH versus Γ_{ads} yielded slopes that were not significantly different from zero. If 2,4-D adsorption resulted from a ligand exchange mechanism, equilibrium pH would have increased with Γ_{ads} because of OH^- release, but this was not observed. This information coupled with the absence of adsorption/desorption hysteresis refute ligand exchange (i.e., inner-sphere complexation) as a likely mechanism for reaction. Therefore, the data suggest that 2,4-D sorption occurs through electrostatic sorption (i.e., outer-sphere complexation or adsorption in the diffuse ion swarm). For example, adsorption may transpire via an anion exchange mechanism:

$$\equiv AlOH_2^+ \text{- - - } Cl^- + R\text{–}COO^- \leftrightarrow \equiv AlOH_2^+ \text{- - - } {}^-OOC\text{–}R + Cl^-. \quad (6)$$

Enhanced 2,4-D adsorption onto mesoporous sorbents might be expected if surface site density were correlated with porosity. However, as indicated by proton titration and ion adsorption measurements, all of these alumina solids have nearly identical Γ_- values (Table 1) at the experimental pH and no differences in surface charge were observed over a wide range in pH [40]. One plausible hypothesis is that sorbate/sorbate interactions may be enhanced within the curved geometry of confining pore walls, relative to external, convex particle surfaces. If 2,4-D sorbs via electrostatic interactions that are supplemented by intermolecular van der Waals forces [31,32,34,38], then it is conceivable that increased sorption results from confining pore geometry that increases probability of interactions between benzene moieties attached to adjacent molecules. This hypothesis is consistent with the FFG isotherm data.

3.3. Bonding of 2,4-D to Al_2O_3 adsorbents

To elucidate the bonding mechanism of 2,4-D on Al_2O_3 surfaces, infrared measurements were made on wet complexes subjected to progressive drying using ATR-FTIR (Figs. 4 and 5). Spectra were obtained for solids reacted for 24 h with an initial 2,4-D concentration of 3.5 mM. The difference spectra (Figs. 4a–4c) obtained by subtracting 0.02 M $CaCl_2$ solution from a slurry of 2,4-D-adsorbent $CaCl_2$ reveals peaks attributable to 2,4-D bond vibrations. Incomplete removal of H_2O bands in the subtraction process hinders observation of asymmetric stretching of the COO^- group (1635 cm^{-1}). Progressive removal of water by purging the sample cell with H_2O- and CO_2-free air increased the resolution of this band with drying time (Figs. 5a–5c). Assignment of additional 2,4-D peaks in the spectra are as follows: C=C aromatic stretching (1480 and 1431 cm^{-1}); symmetric stretch of COO^- (1340 cm^{-1}); and in plane deformation of aromatic C–H (1260 cm^{-1}) [52–55]. Characteristic, but unassigned, 2,4-D peaks are observed at 1615, 1391, and 1290 cm^{-1}. It is apparent that as porosity increases so does the intensity of the unassigned peak at 1615 cm^{-1}, relative to the asymmetric COO^- stretch at 1635 cm^{-1}. Although compelling, we cannot presently attribute this observation to increased inter-molecular interactions within mesopores.

The ATR-FTIR spectra (Figs. 4 and 5) do not show a downward shift in frequency of the asymmetric and symmetric COO^- stretches with adsorption that are indicative of the formation of stable carboxylate complexes with surface coordinated metals (i.e., ligand exchange reactions [56–58]. Thus, the ATR-FTIR and adsorption/desorption data are internally consistent, indicating that 2,4-D binds to both porous and nonporous Al_2O_3 solids via nonspecific (outer-sphere or diffuse swarm) adsorption.

3.4. Mineral transformation during adsorption reactions

Time-dependent changes in mineral structure, specific surface area and porosity were measured over the full range of reaction times employed to evaluate the stability of these materials and to assess whether changes in adsorbent properties might influence contaminant adsorption behavior (Fig. 3, Table 6). The effect of aging on Si adsorbents was not investigated due to the absence of 2,4-D sorption to these materials as discussed previously. After 9 d of reaction, Al-P_{242} (Fig. 3b) begins to show XRD peaks attributable to gibbsite (18°and 20° 2θ) while the other two adsorbents remain relatively unchanged (Figs. 3e and 3h). However, XRD patterns of both mesoporous materials show emergence of

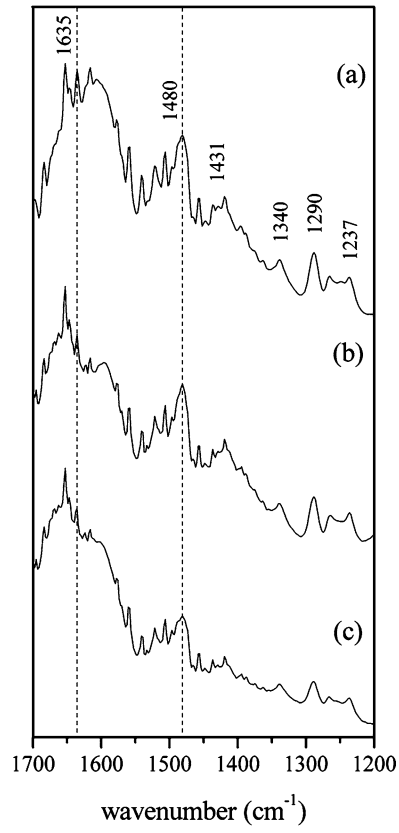

Fig. 4. Attenuated total reflectance-Fourier transform infrared (ATR-FTIR) difference spectra of 2,4-D-adsorbent slurry (0.02 M $CaCl_2$ background electrolyte solution removed): (a) Al-P_{242}, (b) Al-P_{141}, and (c) Al-NP_{37}.

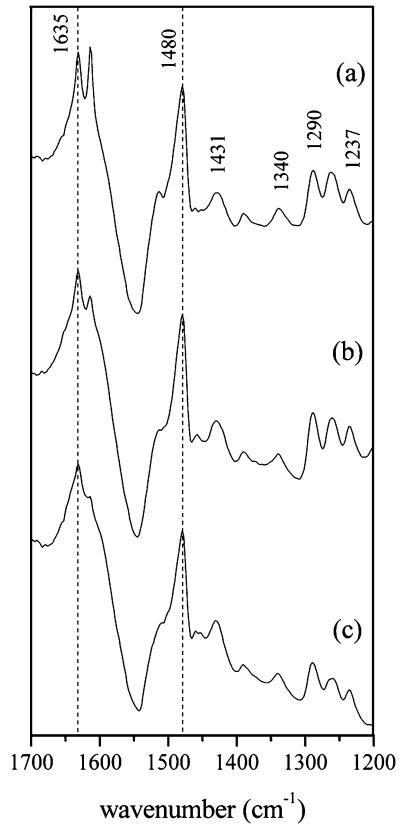

Fig. 5. Attenuated total reflectance-Fourier transform infrared (ATR-FTIR) spectra of 2,4-D-adsorbent slurry after 18 h drying time: (a) Al-P_{242}, (b) Al-P_{141}, and (c) Al-NP_{37}.

gibbsite peaks (Ref. code 07-0324) after 165 d of reaction time (Figs. 3c and 3f).

Thermogravimetric analysis (TGA) was employed to quantify the fraction of solid transformed to gibbsite as a function of starting material and reaction time. The TG-weight loss and endotherm data in the region 250–350 °C were analyzed using the extrapolated onset and return graphical technique [59] (Table 6). The tabulated range includes a lower value, which includes correction for mass loss from unreacted samples over the same temperature range, and a higher value, which is uncorrected for the control (Table 6). Thus, the lower value is a conservative estimate of the mass fraction of gibbsite in product solids formed over the course of the experiment. The data clearly indicate adsorbent transformation to gibbsite, the thermodynamically stable solid [40], over reaction time in suspension.

Goldberg et al. [24] also observed gibbsite formation from less stable amorphous aluminum oxides (S_{BET} ranging from 12.6 to 254 $m^2\,g^{-1}$), using XRD, after 9 d of reaction at pH 4–5. In addition, these authors reported a ninefold decrease in S_{BET} for a sample with an initial $S_{BET} = 254\ m^2\,g^{-1}$. Despite the mineralogical transformation, large changes in S_{BET} (e.g., severalfold decrease) even up to 165 d of reaction were not observed in the present study (Table 6). In addition, D_{pore} as determined by the BJH method did not decrease significantly for the porous materials.

It is noteworthy that, although the mesoporous Al_2O_3 adsorbents showed transformation to more stable solids under the conditions imposed in this study, the materials did not lose their mesoporosity in the process. Despite negligible change in porosity, we did observe a decrease in 2,4-D adsorption at the longest reaction times, particularly for the lowest initial 2,4-D concentration. Further research is needed to facilitate synthesis of kinetically stable mesoporous adsorbents and to determine the conditions suitable for using these materials in contaminant remediation.

4. Summary

Increased intraparticle mesoporosity in Al_2O_3 solids was found to result in increased affinity and uptake of 2,4-D when adsorption was normalized to sorbent surface area. The presence of intraparticle porosity resulted in a statistically significant adsorption enhancement throughout the isotherm for the most porous material (Al-P_{242}) and at the higher concentration range for the solid of intermediate porosity (Al-P_{141}), irrespective of reaction time. In addition to the effects of intraparticle porosity, the positive surface charge of the Al_2O_3 solids (at the experimental pH) contributed to sorptive uptake since no sorption occurred on silica surfaces (very slightly negative to near neutral at the

experimental pH), irrespective of porosity. Adsorption equilibrium is achieved rapidly (<30 min) and reversibly, and sorption appears to be mediated through electrostatic interaction between the dissociated 2,4-D carboxylate group and positively charged surface aluminol groups (outer sphere or diffuse swarm adsorption). These results indicate that even when mineral pores are significantly larger than the adsorbate, they can still impact the energetics of adsorption, possibly by promoting favorable sorbate/sorbate interactions along curved pore walls. Last, XRD and TGA results demonstrate that the mesoporous adsorbents increasingly transform to gibbsite as a function of reaction time in suspension, but that this transformation does not significantly affect sorbent mesoporosity.

Acknowledgments

The authors thank Mary Kay Amistadi for assistance, Drs. Bharat Newalkar and Stephen Stout for mineral synthesis and preparation, Dr. Towhid Hasan and Robin Guynn for performing ICPMS analyses, and Dr. Sunkyung Choi for performing XRD analyses. Financial support was provided by the Penn State Biogeochemical Research Initiative for Education (BRIE) sponsored by NSF (IGERT) Grant DGE-9972759 and the Penn State Materials Research Science and Engineering Center (MRSEC) sponsored by NSF Grant DMR-0080019.

References

[1] L.M. Mayer, Chem. Geol. 114 (1994) 347.
[2] R.G. Luthy, G.R. Aiken, M.L. Brusseau, S.D. Cunningham, P.M. Gschwend, J.J. Pignatello, M. Reinhard, S.J. Triana, W.J. Weber Jr., J.C. Westall, Environ. Sci. Technol. 31 (1997) 3341.
[3] L.M. Mayer, Geochim. Cosmochim. Acta 63 (1999) 207.
[4] J. Farrell, J. Luo, P. Blowers, J. Curry, Environ. Sci. Technol. 36 (2002) 1524.
[5] W.P. Ball, P.V. Roberts, Environ. Sci. Technol. 25 (1991) 1237.
[6] J. Farrell, M. Reinhard, Environ. Sci. Technol. 28 (1994) 53.
[7] J. Farrell, M. Reinhard, Environ. Sci. Technol. 28 (1994) 63.
[8] C.J. Werth, M. Reinhard, Environ. Sci. Technol. 31 (1997) 689.
[9] C.J. Werth, M. Reinhard, Environ. Sci. Technol. 31 (1997) 697.
[10] J. Li, C.J. Werth, Environ. Sci. Technol. 35 (2001) 568.
[11] C.J. Werth, M. Reinhard, Environ, Sci. Technol. 33 (1999) 730.
[12] R. Denoyel, E. Sabio Rey, Langmuir 14 (1998) 7321.
[13] Y.-M. Xu, R.-S. Wang, F. Wu, J. Colloid Interface Sci. 209 (1999) 380.
[14] H. Zhao, K.L. Nagy, J.S. Waples, G.F. Vance, Environ. Sci. Technol. 34 (2000) 4822.
[15] J. Jung, J.-A. Kim, J.-K. Suh, J.-M. Lee, S.-K. Ryu, Water Res. 35 (2001) 937.
[16] M.C. Burleigh, M.A. Markowitz, M.S. Spector, B.C. Gaber, Environ. Sci. Technol. 36 (2002) 2515.
[17] K. Hanna, I. Beurroies, R. Denoyel, D. Desplantier-Giscard, A. Galarneau, F. Di Renzo, J. Colloid Interface Sci. 252 (2002) 276.
[18] Y. Wang, C. Bryan, H. Xu, P. Pohl, Y. Yang, C.J. Brinkert, J. Colloid Interface Sci. 254 (2002) 23.
[19] J.M. Zachara, C.C. Ainsworth, C.E. Cowan, R.L. Schmidt, Environ. Sci. Technol. 24 (1990) 118.
[20] G. Sposito, The Surface Chemistry of Soils, Oxford Univ. Press, New York, 1984.
[21] J.J. Pignatello, Adv. Agron. 69 (2000) 1.
[22] A.M. Mastral, T. García, M.S. Callén, M.V. Navarro, J. Galbán, Environ. Sci. Technol. 35 (2001) 2395.
[23] A.R. Zimmerman, K.W. Goyne, J. Chorover, S. Komarneni, S.L. Brantley, Org. Geochem., in press.
[24] S. Goldberg, I. Lebron, D.L. Suarez, Z.R. Hinedi, Soil Sci. Soc. Am. J. 65 (2001) 78.
[25] L.Y. Chen, S. Jaenicke, G.K. Chuah, Microporous Mater. 12 (1997) 323.
[26] A. Doyle, B.K. Hodnett, Micropor. Mesopor. Mater. 63 (2003) 53.
[27] M.B. McBride, Environmental Chemistry of Soils, Oxford Univ. Press, New York, 1994.
[28] L. Cox, M.C. Hermosín, J. Cornejo, J. Agric. Food Chem. 48 (2000) 93.
[29] J.B. Weber, P.W. Perry, R.P. Upchurch, Soil Sci. Soc. Am. Proc. 29 (1965) 678.
[30] F. Sannino, A. Violante, L. Gianfreda, Pestic. Sci. 51 (1997) 429.
[31] R. Celis, M.C. Hermosín, L. Cox, J. Cornejo, Environ. Sci. Technol. 33 (1999) 1200.
[32] D. Vasudevan, E.M. Cooper, O.L. Van Exem, Env. Sci. Technol. 36 (2002) 501.
[33] J.R. Watson, A.M. Posner, J.P. Quirk, J. Soil Sci. 24 (1973) 503.
[34] B.V. Kavanagh, A.M. Posner, J.P. Quirk, J. Colloid Interface Sci. 61 (1977) 545.
[35] P. Benoit, E. Barriuso, S. Houot, R. Calvet, Eur. J. Soil Sci. 47 (1996) 567.
[36] M.Q. Hu, M.L. Brusseau, Environ. Toxicol. Chem. 17 (1998) 1673.
[37] L. Guo, W.A. Jury, R.J. Wagenet, M. Flury, J. Contam. Hydrol. 43 (2000) 45.
[38] B.V. Kavanagh, A.M. Posner, J.P. Quirk, J. Soil Sci. 31 (1980) 33.
[39] R. Haque, R. Sexton, J. Colloid Interface Sci. 27 (1968) 818.
[40] K.W. Goyne, A.R. Zimmerman, B.L. Newalkar, S. Komarneni, S.L. Brantley, J. Chorover, J. Porous Mater. 9 (2002) 243.
[41] S. Komarneni, R. Pidugu, V.C. Menon, J. Porous Mater. 3 (1996) 99.
[42] P.T. Tanev, T.J. Pinnavaia, Science 267 (1995) 865.
[43] W. Zhang, T.R. Pauly, T.J. Pinnavaia, Chem. Mater. 9 (1997) 2491.
[44] K.S.W. Sing, D.H. Everett, R.A.W. Haul, L. Moscou, R.A. Pierotti, J. Rouquerol, T. Siemieniewska, Pure Appl. Chem. 57 (1985) 603.
[45] E.P. Barrett, L.J. Joyner, P.P. Helenda, J. Am. Chem. Soc. 73 (1951) 373.
[46] G.D. Halsey, J. Chem. Phys. 16 (1948) 931.
[47] B. Xing, J.J. Pignatello, Environ. Sci. Technol. 15 (1996) 1282.
[48] W. Stumm, Chemistry of the Solid–Water Interface, Wiley, New York, 1992.
[49] G. Sposito, The Chemistry of Soils, Oxford Univ. Press, New York, 1989.
[50] R. Fowler, E.A. Guggenheim, Statistical Thermodynamics, Cambridge Univ. Press, London, 1965.
[51] S. Trasatti, Electroanal. Chem. 53 (1974) 335.
[52] A.U. Baes, P.R. Bloom, Soil Sci. Soc. Am. J. 53 (1989) 695.
[53] R.M. Silverstein, G.C. Bassler, T.C. Morrill, Spectrometric Identification of Organic Compounds, fifth ed., Wiley, New York, 1991.
[54] M.C. Hermosin, J. Cornejo, J. Environ. Qual. 22 (1993) 325.
[55] J.I. Pérez-Martínez, J.M. Ginés, E. Morillo, M.L.G. Rodríguez, J.R. Moyano, Environ. Technol. 21 (2000) 209.
[56] B. Gu, J. Schmitt, Z. Chen, L. Liang, J.F. McCarthy, Geochim. Cosmochim. Acta 59 (1995) 219.
[57] J. Chorover, M.K. Amistadi, Geochim. Cosmochim. Acta 65 (2001) 95.
[58] K. Vermöhlen, H. Lewandowski, H.-D. Narres, E. Koglin, Colloids Surf. A 170 (2000) 181.
[59] A.D. Karathanasis, W.G. Harris, in: J.E. Amonette, L.W. Zelanzy (Eds.), Quantitative Methods in Soil Mineralogy, SSSA, Madison, WI, 1994, p. 360.